*sensors*

*Article*

# Cu$_2$O and Au/Cu$_2$O Particles: Surface Properties and Applications in Glucose Sensing

**Yu-Ho Won [1] and Lia A. Stanciu [1,2],***

[1]  School of Materials Engineering, Purdue University, West Lafayette, IN 47907, USA;
    E-Mail: ywon@purdue.edu
[2]  Birck Nanotechnology Center, Purdue University, West Lafayette, IN 47907, USA

**\*** Author to whom correspondence should be addressed; E-Mail: lstanciu@purdue.edu;
    Tel./Fax: +1-765-496-3552.

**Abstract:** In this work we investigated the surface and facet-dependent catalytic properties of metal oxide particles as well as noble metal/metal oxide heterogeneous structures, with cuprous oxide (Cu$_2$O) and Au/Cu$_2$O being selected as model systems. As an example of application, we explored the potential of these materials in developing electrocatalytic devices. Cu$_2$O particles were synthesized in various shapes, then used for testing their morphology-dependent electrochemical properties applied to the detection of glucose. While we did not attempt to obtain the best detection limit reported to date, the octahedral and hexapod Cu$_2$O particles showed reasonable detection limits of 0.51 and 0.60 mM, respectively, which are physiologically relevant concentrations. However, detection limit seems to be less affected by particle shapes than sensitivity. Heterogeneous systems where Au NPs were deposited on the surface of Cu$_2$O particles were also tested with similar results in terms of the effect of surface orientation.

## 1. Introduction

In this work we investigated the surface and facet-dependent catalytic properties of metal oxide particles as well as noble metal/metal oxide heterogeneous structures, with cuprous oxide (Cu$_2$O) and

Au/Cu$_2$O being selected as model systems. As an example of application, we explored the potential of these materials in developing electrocatalytic devices.

While conventional methodologies of material synthesis and processing have been developed in the past decades to a level allowing production of an enormous range of sophisticated products, pushing the state of the art forward requires understanding of current materials from new, still unexplored, perspectives. In the recent years, many studies have been carried out on size and shape control of inorganic crystals [1–10]. Now that the capacity to control shape of various particles has been established, there is a need to extend beyond synthesis and characterization of their physical and chemical properties into more rational and systematic studies on how these advances on shape and morphology control can be harvested towards the next leap in the state of the art of their applications. Systematically correlating the surface, interfacial and facet dependent properties with the discovery of new materials and their implementation into applications, such as photocatalytic or electrocatalytic devices, holds promise for the engineering of the next generation of materials with superior, not previously attained properties. To rationally design materials with built-in photocatalytic and electrocatalytic activity tailored to address emerging environmental and biomedical challenges (e.g., how to design custom materials used to decompose organic pollutants of any chemical structure), there is a need to understand how the facet dependent properties of metal oxide particles affect their catalytic activity. While there has been much research in the area of material synthesis at different scale lengths, there is not much attention given to the investigation of facet-dependent properties of shape-controlled metal oxide crystals to date. For example, a lot of attention has been given to measurements of electrical properties of nanowires [11–15], or the catalytic properties of spherical nanoparticles [16–18], but the effect of facet surface in Cu$_2$O nanocrystals and/or particles with controlled shapes (e.g., cubic, octahedron, truncated octahedron or hexapod) has not been largely or systematically investigated. Synthesis of shape controlled Cu$_2$O nano- and micro-crystals has already been performed [19–28], however not much attention has been given to actually exploiting this well established capacity to control this material's shape and surface properties for any biosensing or biocatalytic applications. In this work, we performed experiments that work towards closing this knowledge gap by focusing on Cu$_2$O as a model metal oxide that has promising electrical characteristics, photocatalytic properties, and that is amenable to shape-controlled synthesis, but for which very little is known about the mechanisms involved during its use in electrocatalysis. Such metal oxides are interesting substitutes for noble metal catalysts owing to their lower cost, coupled with a significant catalytic activity. Among semiconductor materials, Cu$_2$O has attracted intensive attention because it can be used in various devices, such as photoelectrochemical cells, sensors, catalysts, and batteries [7–10]. The morphology of Cu$_2$O can be adjusted to tailor its properties to the requirements of each application. The surfaces of Cu$_2$O crystals showing different morphology are exposed with different crystallographic planes. For example, the {100} crystallographic planes are exposed in the Cu$_2$O cube, while the {111} planes are exposed in the Cu$_2$O octahedron. These surfaces have different atomic arrangements and different surface energies, and thus they are expected to induce different physical and chemical properties.

This work establishes an understanding of the correlation between the facet-dependent properties of shape-controlled metal oxides and their resulting catalytic properties. We focused our initial work on Cu$_2$O particles as a well studied model, identified the nature of reactive species involved, and established the mechanism of action. The results also determined the way that shape, surface

orientation and interfacial reactivity of $Cu_2O$ particles affect the catalytic properties and how these can be exploited in practical devices and applications. As an example of application that will have both relevance to human health and the capacity to highlight the surface-dependent properties of differently shaped crystals glucose detection was performed. The knowledge acquired can impact the environmental and biomedical fields, and industries that are heavily using catalyst technologies.

## 2. Experimental Section

### 2.1. Materials

To synthesize $Cu_2O$ and Au decorated $Cu_2O$ (Au/$Cu_2O$) particles, $CuCl_2$, NaOH, sodium dodecyl sulfate (SDS), $NH_2OH \cdot HCl$, and $HAuCl_4$ were purchased from Sigma Aldrich (St. Louis, MO, USA). D-(+)-Glucose, $K_4Fe(CN)_6$, and $K_3Fe(CN)_6$ for the glucose sensor tests and $KH_2PO_4$ and $K_2HPO_4$ for the preparation of the phosphate buffer solution (PBS) were also obtained from Sigma Aldrich.

### 2.2. Synthesis of $Cu_2O$ and Au/$Cu_2O$ Nanoparticles

$Cu_2O$ particles with various morphologies such as cube, truncated octahedron, octahedron, and hexapod were synthesized according to the report by Ho and Huang [9]. For the preparation of cubic $Cu_2O$ particles, 0.1 mL of 0.1 M $CuCl_2$ was injected into 9.5 mL of deionized (DI) water. One M NaOH (0.2 mL) and SDS (surfactant, 0.087 g) were added into the $CuCl_2$ solution under vigorous stirring. After dissolution of SDS, 0.1 mL of 0.2 M $NH_2OH \cdot HCl$ was added in the mixed solution. The solution was stirred at 800 rpm for 2 h for aging. The solution was centrifuged and washed by ethanol at 5,000 rpm for 5 min to remove unreacted chemicals. Finally, $Cu_2O$ particles were dispersed in ethanol. $Cu_2O$ particles with various shapes were obtained by control of amounts of DI water, NaOH, and $NH_2OH \cdot HCl$ as shown in Table 1. Au/$Cu_2O$ particles were prepared by adding $HAuCl_4$ solution in the $Cu_2O$ colloid solution [29]. A volume of 50 μL of 1.2 mM $HAuCl_4$ was injected into 150 μL of $Cu_2O$ colloid solution dispersed in DI water under stirring at 600 rpm. After stirring for 2 min, the mixed solution was centrifuged and washed by ethanol two times. Finally, Au/$Cu_2O$ particles were dispersed in ethanol. In this reaction, a reductant for Au is not required because $AuCl_4^-$ ions reduced by $Cu_2O$. The reaction is as follows [29]:
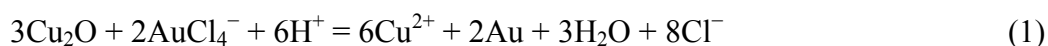
$$3Cu_2O + 2AuCl_4^- + 6H^+ = 6Cu^{2+} + 2Au + 3H_2O + 8Cl^- \tag{1}$$

**Table 1.** Raw materials for the synthesis of $Cu_2O$ particles.

|  | Cubes | Truncated octahedra | Octahedra | Hexapods |
|---|---|---|---|---|
| **DI water** | 9.5 mL | 9.2 mL | 9.0 mL | 9.05 mL |
| **0.1 M CuCl₂** | 0.1 mL | 0.1 mL | 0.1 mL | 0.1 mL |
| **1.0 M NaOH** | 0.3 mL | 0.3 mL | 0.3 mL | 0.2 mL |
| **SDS** | 0.087 g | 0.087 g | 0.087 g | 0.087 g |
| **0.2 M NH₂OH·HCl** | 0.1 mL | 0.4 mL | 0.6 mL | 0.65 mL |

*2.3. Apparatus and Measurements*

Scanning electron microscopy (SEM) images of $Cu_2O$ and $Au/Cu_2O$ particles were obtained using a XL 40 (FEI) instrument operating at 10 kV. The X-ray diffraction (XRD) patterns of the particles were measured with a Bruker D8 focus (Cu Kα radiation, λ = 1.5406 Å). The electrochemical measurements of the sensors for the detection of glucose were performed with an epsilon C3 cell stand (BASi). A conventional three-electrode system, which consists of screen printed electrode (SPE, area = $4 \times 5$ $mm^2$, Pine Research Instrumentation, Durham, NC, USA) as a working electrode, Pt wire as a counter electrode, and Ag/AgCl electrode as a reference electrode, was used for the sensor measurements.

*2.4. Preparation and Characterization of the Sensors*

As an example of application that has the potential to highlight the surface-dependent properties of differently shaped crystals, an electrochemical biosensing configuration in which $Cu_2O$ is the main sensing element was tested. The as-synthesized $Cu_2O$ particles were coated on commercially available screen printed electrodes (SPE). $Cu_2O$ particles dispersed in ethanol were dropped on the surface of SPEs and dried for 1 h at 25 °C. A PBS solution (0.1 M) containing $KH_2PO_4$ and $K_2HPO_4$ was prepared. Amperometric responses of the sensors were obtained in 3 mL of PBS (0.1 M) containing 5 mM $[Fe(CN)_6]^{3-}$ by adding glucose solution, under magnetic stirring (150 rpm). The current response of amperometric sensors usually depends on the applied potential and pH value of buffer solution. To optimize the current response of the sensor, the effects of an applied potential and a pH of the buffer solution were investigated. To confirm reproducibility of electrodes, we prepared three of the same electrodes and measured the current response three times. The pH value of the buffer solution was adjusted from 5 to 10 by adding HCl and NaOH to the buffer solution. To obtain the detection limit, the current responses of the sensor were measured by adding 1 mM glucose successively into the same measuring cell, under optimum conditions.

## 3. Results and Discussion

It is important to note that the current work doesn't aim to obtain the best sensor performance reported, but to verify the hypothesis that the surface properties of variously shaped particles influence their catalytic efficiency in both metal oxide particles, as well as in noble metal/metal oxide heterogeneous structures, with $Cu_2O$ and $Au/Cu_2O$ being selected as model systems. As an example of application, we explored the potential of these materials in developing electrocatalytic devices. To test this hypothesis, the morphology-dependent electrocatalytic properties were evaluated for both systems.

$Cu_2O$ particles having various shapes were prepared in house, according to the reported method by Ho and Huang [9]. The amounts of precursor materials such as NaOH and $NH_2OH \cdot HCl$ were modified from the reported method to obtain well defined shapes as shown in Table 1.

Figure 1 shows SEM images of synthesized cubic, truncated octahedral, octahedral, and hexapod $Cu_2O$ particles. The sizes of the particles regardless of shapes are in the range of 800 nm–1 μm. Cubic $Cu_2O$ particles Figure 1(a) have all six {100} faces and truncated octahedral $Cu_2O$ particles Figure 1(b) have six {100} faces and eight {111} faces. Octahderal Figure 1(c) and hexapod Figure 1(d) $Cu_2O$

particles have eight and twenty four {111} faces, respectively. Thus, the effects of crystal facets of Cu₂O particles on biosensing properties can be tested.

**Figure 1.** SEM images of synthesized Cu₂O particles (**a**) Cubes; (**b**) Truncated octahedral; (**c**) Octahedra; and (**d**) Hexapods (Scale bar: 1 μm).
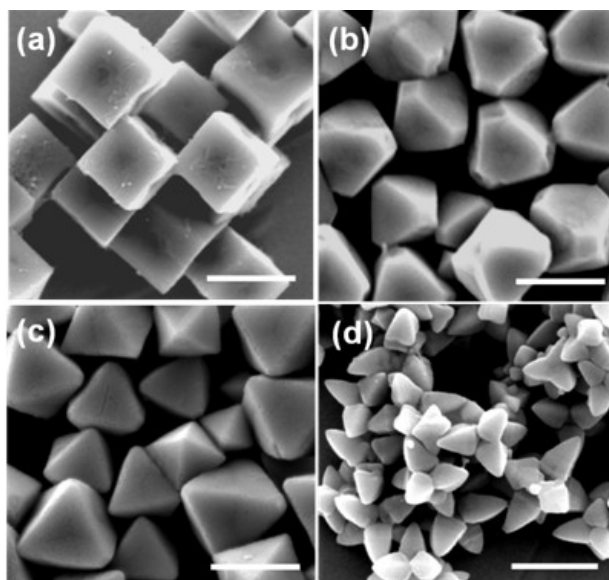


The phase of synthesized particles was confirmed by the XRD measurement. The colloids of octahedral Cu₂O particles were dropped on the slide glass and dried at room temperature. Cubic and octahedral Cu₂O particles show similar XRD patterns as shown in Figure 2. The relative intensities of {111} and {200} reflections provide information regarding the crystal orientation against the substrate.

**Figure 2.** Representative XRD patterns of cubic and octahedral Cu₂O particles.
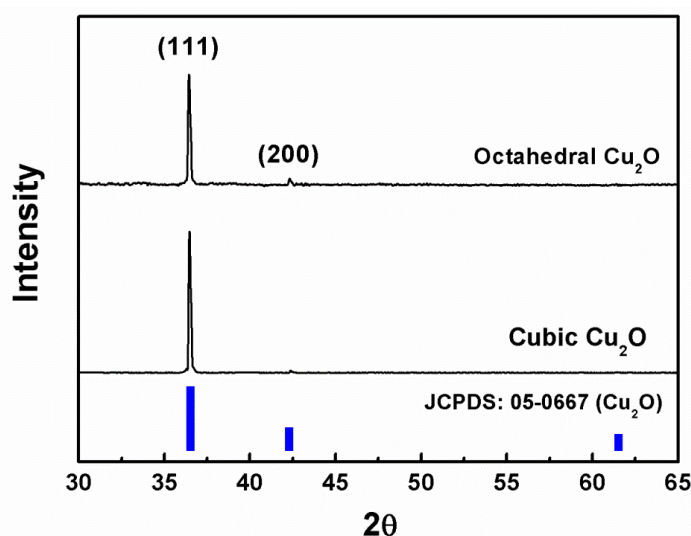


As an example of application that is suitable for verifying the hypothesis that different surface crystallographic orientations will affect the particles' catalytic performance, the effect of Cu₂O particles' morphologies on their potential to be used in enzyme-free electrochemical glucose sensor configurations was chosen. Figure 3 shows a schematic of Cu₂O-based enzyme-free glucose sensors.

**Figure 3.** Schematic of $Cu_2O$-based electrochemical enzyme-free glucose biosensor.
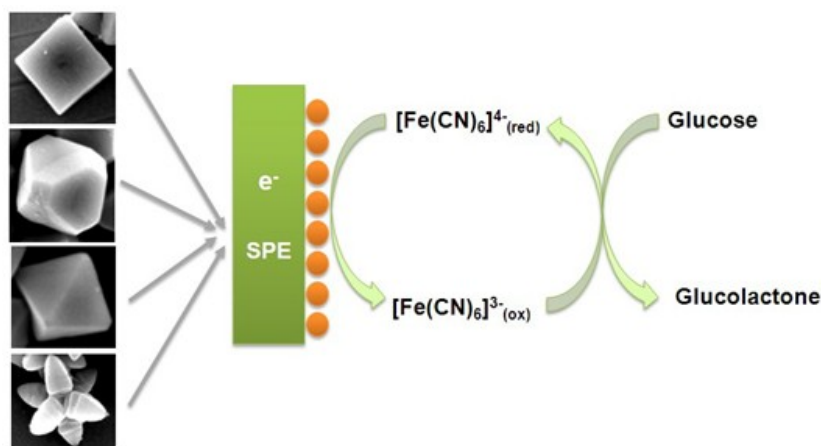


To investigate their morphology-dependent electrochemical properties, electrodes coated with cubic, truncated octahedral, octahedral, and hexapod $Cu_2O$ particles were prepared. The electrode current responses were measured via a three-electrode system in 0.1 M PBS containing 5 mM $[Fe(CN)_6]^{3-/4-}$ as an electron mediator. Glucose added to the PBS solution is oxidized to glucolactone by the electron mediator. The amperometric current, generated through this reaction, is indicative of the presence of glucose. Figure 4 shows cyclic voltammograms (CVs) of the bare SPE and the SPE with hexapod $Cu_2O$ particles in 0.1 M PBS at a scan rate of 100 mV/s.

**Figure 4.** CVs of bare SPE and SPE with hexapod $Cu_2O$.
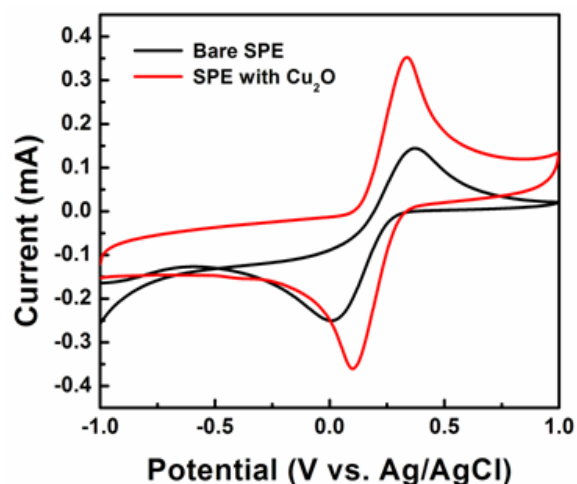


The redox peaks corresponding to $[Fe(CN)_6]^{3-/4-}$ couple occur at 330 and 100 mV. The redox peaks of the SPE with $Cu_2O$ particles show higher intensities than those of the bare electrodes. This shows that $Cu_2O$ particles hold promise to offer some effectiveness of the enzyme-free sensors based on these materials.

The current sensitivity of amperometric sensors is influenced by the applied potential and the pH value of the buffer solution. These variables were optimized to achieve the maximum sensitivity of the sensor. Figure 5 shows the effect of pH values of test PBS solution on the current response at a constant concentration of glucose (5 mM).

**Figure 5.** Amperometric responses of the electrode with $Cu_2O$ to various pH values of PBS (0.1 M) containing 5 mM $[Fe(CN)_6]^{3-/4-}$ at 50 mV to 5 mM glucose.
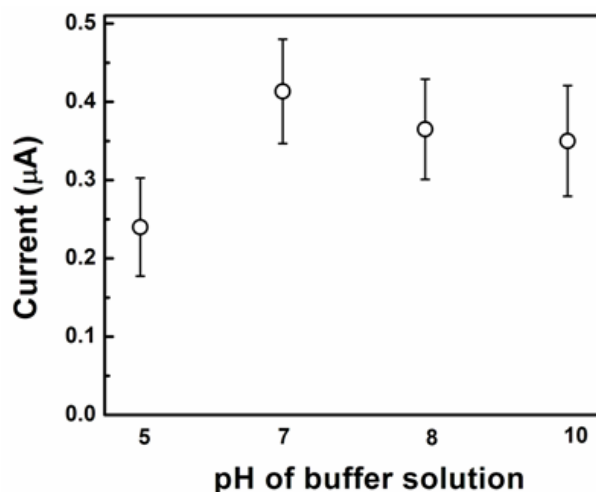


The highest current response was registered at a pH value of 7. To optimize the applied potential three identical electrodes of each particle shape were tested three times at applied potential values ranging from 50 to 400 mV as shown in Figure 6. The maximum value of the current response was registered at 50 mV. These optimized values for pH and applied potential were used for all subsequent testing. To investigate the morphology-dependent electrochemical abilities of the $Cu_2O$ particles, electrodes coated with $Cu_2O$ particles of different shapes (cube, truncated octahedron, octahedron, and hexapod) were prepared.

**Figure 6.** Amperometric responses of the electrode with $Cu_2O$ to various potential (mV *vs.* Ag/AgCl) of PBS (0.1 M) containing 5 mM $[Fe(CN)_6]^{3-/4-}$ to 5 mM glucose.
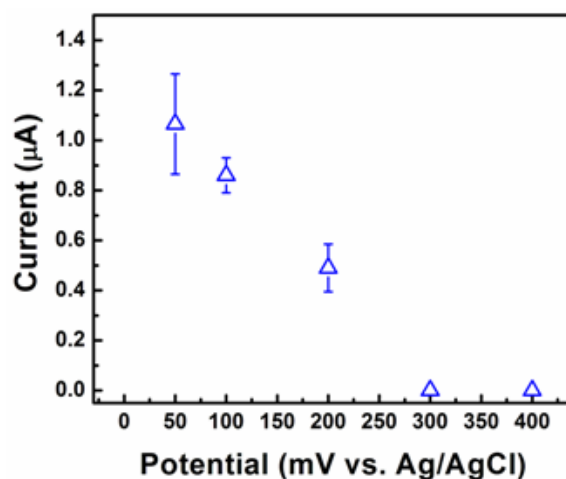


Figure 7 shows the current responses of these electrodes when glucose was introduced in the system. The current responses were measured three times in 0.1 M PBS containing 5 mM $[Fe(CN)_6]^{3-/4-}$ at 50 mV and in the presence of 5 mM glucose. The octahedral and hexapod $Cu_2O$ particles have the {111} crystallographic planes exposed at their surface, while the cubic $Cu_2O$ particles have the {100} crystallographic planes exposed at their surface.

**Figure 7.** Amperometric responses of electrodes coated with $Cu_2O$ particles with various morphologies in 0.1 M PBS containing 5 mM $[Fe(CN)_6]^{3-/4-}$ at an applied potential of 50 mV in the presence of 5 mM glucose.
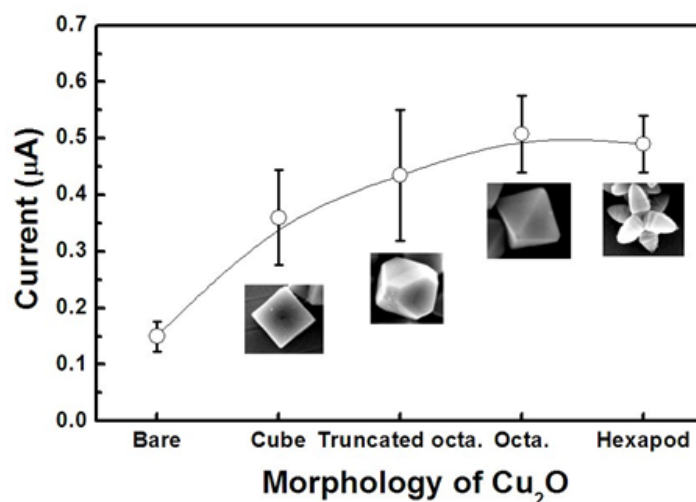


The results show that the {111} crystallographic orientation is more advantageous in terms of current response than the 100} crystallographic orientation. Interestingly the truncated octahedral $Cu_2O$ particles, which have both {111} and {100} crystallographic planes exposed at their surface showed a higher current response than the cubic $Cu_2O$ particles, but somewhat lower than the octahedral and hexapod shaped particles. It can thus be stated that the current responses of the electrodes increase with the area occupied by {111} planes. This finding shows that the {111} crystallographic planes are more effective than the {100} crystallographic planes for catalyzing the electrochemical enzyme free reactions involved in the glucose detection. In these reactions, $Cu_2O$ particles enhance the electron transfer. It is thus safe to say that the specific electrical conductivity of each shape is affecting the sensitivity of the electrochemical sensing, where electron transfer is critical. From the sensitivity results, we can conclude that the electrical conductivity of the {111} planes is higher than that of the {100} planes in $Cu_2O$ particles. This result is in good agreement with the report by Kuo *et al.*, in which the authors used *I–V* measurements to show that the {111} facets are more conductive than {100} facets in $Cu_2O$ particles [30].

Figure 8(a,c) show the amperometric current *vs.* time curves of octahedral and hexapod $Cu_2O$-based electrodes, respectively. The current responses were measured by adding 1 mM glucose successively into the test PBS solution containing 5 mM $[Fe(CN)_6]^{3-/4-}$ at an applied potential of 50 mV. Figure 4(b,d) show the calibration plots with linear regression analysis from Figure 8(a,c), respectively. The current responses of both SPEs showed linear relationships with the concentration of glucose (1–14 mM). The detection limits of SPEs coated with octahedral and hexapod $Cu_2O$ particles were 0.51 and 0.60 mM of glucose, respectively, determined from the linear graph (signal-to-noise ratio = 3). While the performance of these electrodes are not the best on the market the detection limts are still smaller than the range of physiological blood glucose concentration (2–10 mM). We can conclude that indeed, crystallographic orientation of the facets has an effect on both detection limit and sensitivity, however the sensitivity is affected to a larger extent by crystallographic orientation.

**Figure 8.** (**a**)/(**c**) Amperometric responses and (**b**)/(**d**) calibration plots (current *vs.* concentration of glucose) with linear regression analysis of octahedral (**a**,**c**) and hexapod (**b**,**d**) Cu$_2$O-based electrodes in 0.1 M PBS containing 5 mM [Fe(CN)$_6$]$^{3-/4-}$ at an applied potential of 50 mV with successive additions of 1 mM glucose.
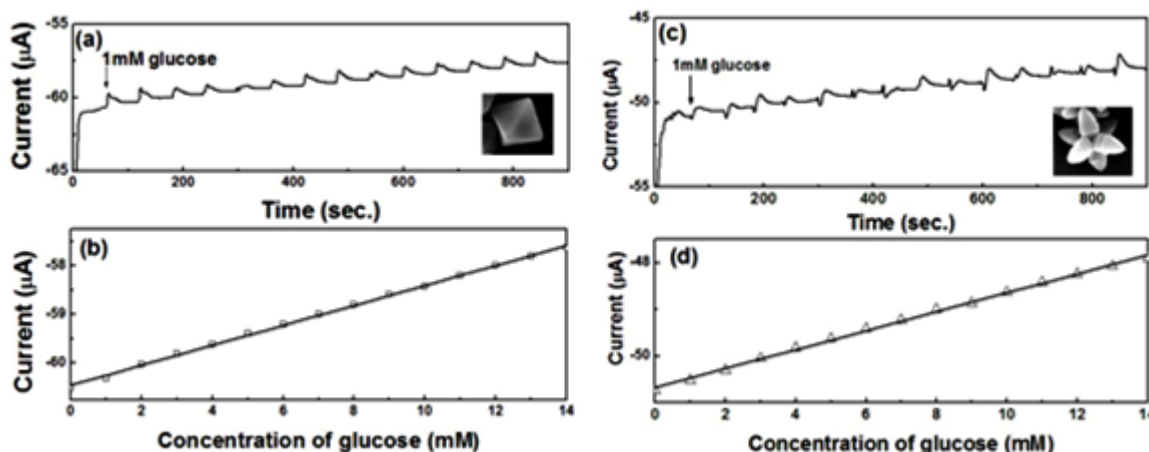


The next question to be answered relates to whether or not doping of metal oxides with noble metals will significantly influence the effect of surface properties of the substrate oxide on the overall doped material electrochemical and catalytic properties. Electrodes modified of Au NPs have been researched as for the non-enzymatic electrochemical detection of glucose [31,32]. We fabricated heterogeneous Au/Cu$_2$O particles and evaluated their facet-dependent properties by using similar methods as for bare Cu$_2$O particles. Our hypothesis was that the catalytic activity of metal oxides can be enhanced by doping with noble metals, but how does this change with the exposure of various crystallographic planes in Cu$_2$O?

We eliminated the need of an electron mediator from the electrochemical sensing configurations, once Au NPs were decorated on the surface of Cu$_2$O particles [29]. Au NPs were synthesized on the surface of Cu$_2$O particles through the reduction of AuCl$_4^-$ anions by Cu$_2$O, according to Equation (1). Figure 9 shows SEM images of cubic (a,d), octahedral (b,e), and hexapod (c,f) Cu$_2$O particles before and after Au decorating.

To test the hypothesis that Au doping of Cu$_2$O will enhance their electrocatalytic properties and capacity to be incorporated in enzyme-free electrochemical sensing configuration, Au/Cu$_2$O particles were deposited on screen printed electrodes and tested for the detection of glucose. Since Cu$_2$O alone did not seem to offer the best detection limit for glucose, the next question to be answered was whether or not synergistically combining the good electrocatalytic ability towards glucose oxidation of Au NPs, with the good electrical conductivity of Cu$_2$O particles with {111} faces will lead to significant improvements in this area. The answer to this question will be significant from the point of view of understanding how doping with noble metals might influence oxides' performance and whether or not the initial shape effects are still maintained. Figure 10 shows the CVs of the SPE with Au decorated hexapod Cu$_2$O in 0.5 M NaOH solution in the absence and presence of glucose (10, 20, and 50 mM) at a scan rate of 10 mV/s.

**Figure 9.** SEM images of (**a**) cubic Cu₂O; (**b**) octahedral Cu₂O; (**c**) hexapod Cu₂O; (**d**) cubic Au/Cu₂O; (**e**) octahedral Au/Cu₂O; and (**f**) hexapod Au/Cu₂O.
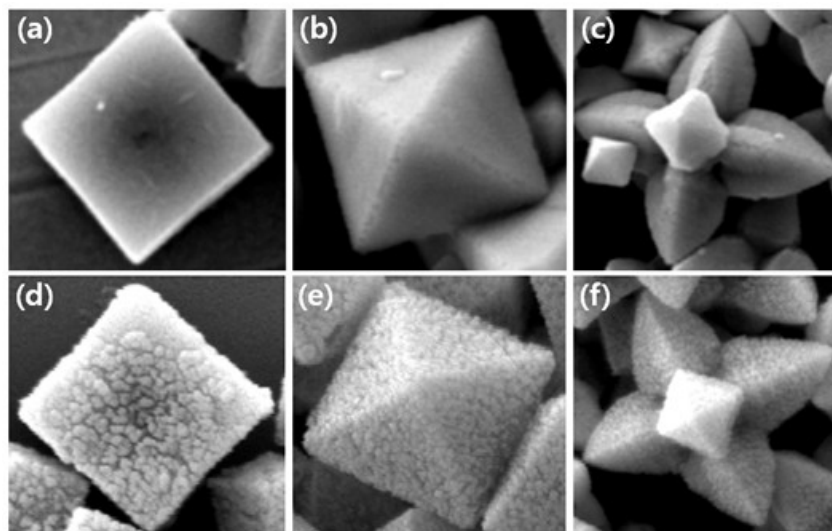


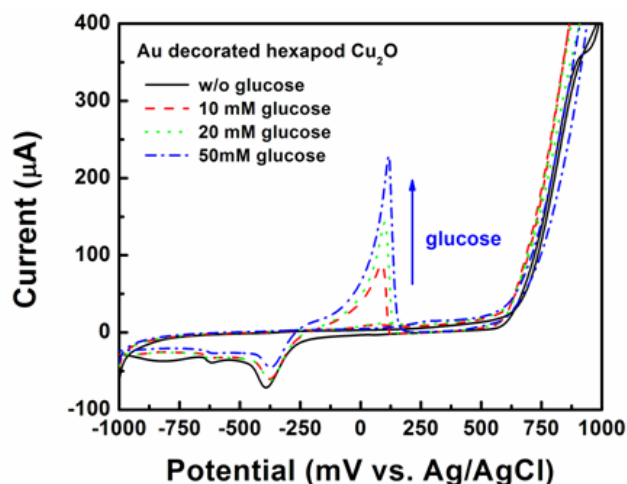**Figure 10.** Cyclic voltammograms of hexapod Au/Cu₂O-based electrode in 0.5 M NaOH with additions of 0, 10, 20, and 50 mM glucose at a scan rate of 10 mV/s.



It is obvious that the SPE shows no peak corresponding to glucose oxidation (the black solid line in Figure 6). In the presence of glucose, the electrode shows the indicative peak of glucose oxidation at 100 mV. As the glucose concentration increased from 10 to 50 mM, the peak intensity also increased. On the other hand, the peak currents corresponding to AuOH reduction at −350 mV decreased, due to the fact that certain amounts of AuOH were used for glucose oxidation as the glucose concentration increased [32].

In the next step, the influence of the crystallographic orientation of Cu₂O particles in the Au/Cu₂O configuration, on the effectiveness of glucose oxidation was investigated. Figure 11 shows CVs of SPEs coated with Au decorated cubic, octahedral, and hexapod Cu₂O, which were tested in 0.5 M NaOH solution, and in the presence of 10 mM glucose. The octahedral and hexapod Au/Cu₂O particles showed higher peak currents than the cubic Au/Cu₂O particles. This is following the same trends described above for bare Cu₂O particles, in terms of the influence of the conductivities of {111} and {100} facets.

**Figure 11.** Cyclic voltammograms of electrodes coated with Au decorated cubic, octahedral, and hexapod $Cu_2O$ in 0.5 M NaOH solution in the presence of 10 mM glucose and corresponding SEM images of the particles.
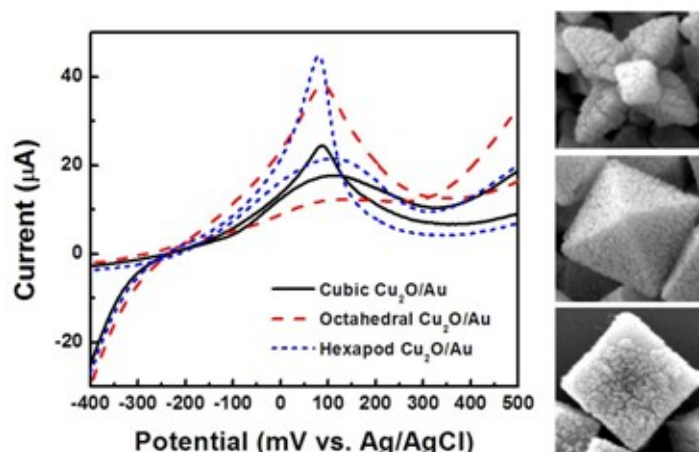


To identify the peak corresponding to the glucose oxidation, cyclic voltammograms coated with Au decorated hexapod $Cu_2O$ particles, Au nanoparticles, and uncoated hexapod $Cu_2O$ were tested. The testing solution contained 0.5 M NaOH and 10 mM glucose as shown in Figure 12. While the electrodes with hexapod $Cu_2O$ particles showed no peak for glucose oxidation given the absence of an electron mediator, the electrodes with Au NPs and $Au/Cu_2O$ particles showed peaks corresponding to glucose oxidation at 100 mV. The peak current corresponding to $Au/Cu_2O$ was higher than that corresponding to only Au nanoparticles. This indicates that the best electrochemical performance is offered by doping $Cu_2O$ particles with Au rather than using Au nanoparticles alone. As mentioned above, the current response of amperometric devices is affected by the applied potential. To find the optimum potential, the current responses of electrodes coated with $Au/Cu_2O$ particles were obtained at applied potentials ranging from −700 to 700 mV.

**Figure 12.** Cyclic voltammograms of electrodes coated with hexapod $Au/Cu_2O$ particles, Au nanoparticles, and hexapod $Cu_2O$ in 0.5 M NaOH solution, and in the presence of 10 mM glucose and corresponding SEM images of the particles.
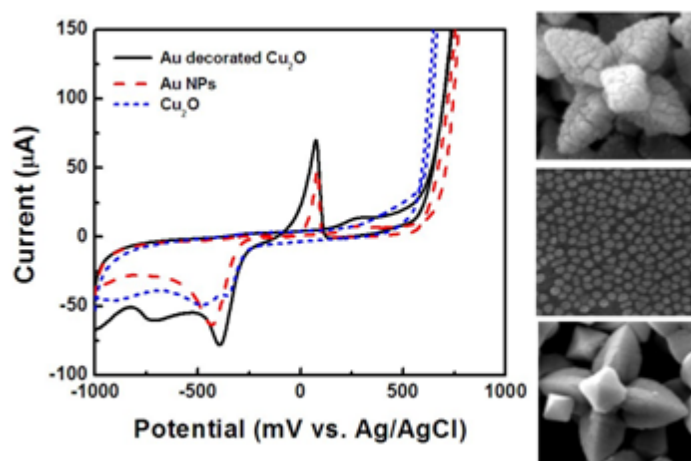
The current response of the SPEs showed the highest value at −600 mV (data not shown). Thus, Au/Cu$_2$O-based enzyme-free glucose sensors were tested at −600 mV. Figure 13(a,b) show the amperometric responses *vs.* time curve and the calibration plot, respectively, of the electrode coated with hexapod Au/Cu$_2$O particles in 0.5 M NaOH, at an applied potential of −600 mV, with successive additions of 1 mM glucose.

**Figure 13.** (**a**) Amperometric responses and (**b**) calibration plot (current *vs.* concentration of glucose) with linear regression analysis of hexapod Au/Cu$_2$O-based electrodes in 0.5 M NaOH at an applied potential of −600 mV and with successive additions of 1 mM glucose.
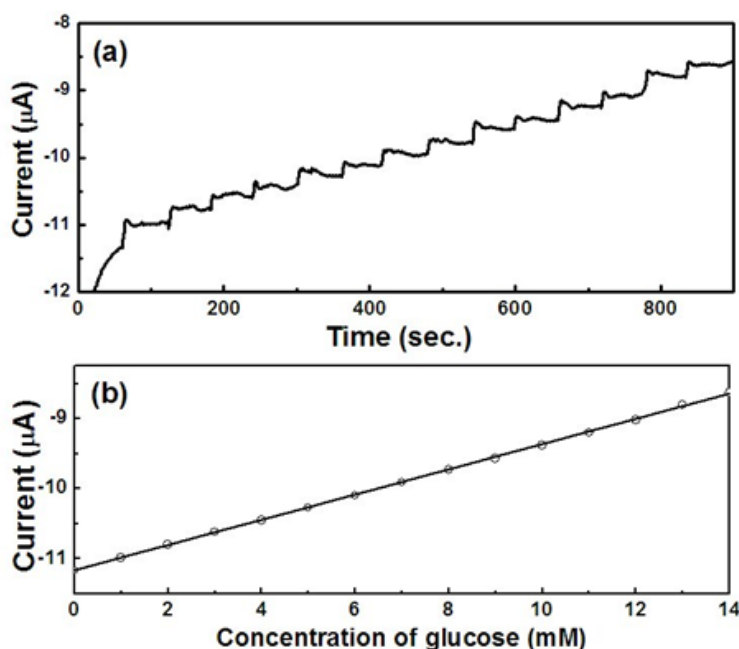


The current responses are linear with the glucose concentration in a wide range from 1 to 14 mM ($R^2$ = 0.999). The detection limit of the sensor based on Au/Cu$_2$O particles were 0.21 mM glucose, which is lower than that for the undoped hexapod Cu$_2$O particles (detection limit = 0.6 mM), determined from the linear graph (signal-to-noise ratio = 3). We can conclude that the experimental results converge to the idea that the exposure of {111} planes in Cu$_2$O particles, together with Au doping is the most effective configuration from the point of view of the electrocatalytical properties. This is due to synergistic effects brought in by the increased conductivity of Cu$_2$O {111} crystallographic planes, coupled with the enhanced electron transfer capabilities of Au NPs. While our results established that the shape and facet crystallographic orientation indeed plays a role on the materials' electrocatalytic activity in both doped and un-doped oxides, the inherent redox properties still maintain the dominant influence. Having the capacity to control the shapes and surface orientation of various oxide particles can lead to opportunities in fine tuning certain properties, especially those that are affected by the electrical conductivity.

## 4. Conclusions

Cu$_2$O and Au/Cu$_2$O particles of various shapes (cube, truncated octahedron, octahedron, and hexapod) were synthesized and their morphology-dependent electrochemical properties were tested in

an example configuration set up for the detection of glucose. The octahedral and hexapod $Cu_2O$ that have a {111} crystallographic orientation exposed at their surface, showed improved electrocatalytical properties than the cubic $Cu_2O$, which have {100} orientations exposed at their surface. This suggests that the {111} orientations are more electrical conductive than the {100} facets in $Cu_2O$ particles. While we did not attempt to obtain the best glucose sensing on the market, but to merely use glucose sensing as a well studied model, the electrodes fabricated with octahedral and hexapod $Cu_2O$ particles showed detection limits of physiological relevance concentrations. While the detection limit is slightly affected particle orientation, there is a larger effect on the sensitivity. Heterogeneous systems where Au NPs were deposited on the surface of $Cu_2O$ particles were also tested. The hypothesis that surface orientation influences observed in the electrochemical configuration with solely $Cu_2O$ particles maintained in $Au/Cu_2O$ systems was tested. These materials showed that the hexapod shape of $Au/Cu_2O$ synergetically combined the effect of the electrocatalytic ability towards glucose oxidation of Au NPs, with the increased electrical conductivity of {111} facets of the hexapod $Cu_2O$ particles. While the inherent physical and chemical properties of the materials themselves maintain the dominant role in their electrocatalytic capacity, having the opportunity to control the shapes and surface orientation of various particles can assist in fine tuning certain properties, especially those where the electrical conductivity is critical.

## Acknowledgements

## References

1. Seo, D.; Yoo, C.I.; Park, J.C.; Park, S.M.; Ryu, S.; Song, H. Directed surface overgrowth and morphology control of polyhedral gold nanocrystals. *Angew. Chem. Int. Ed.* **2008**, *47*, 763–767.
2. Xia, Y.; Xiong, Y.J.; Lim, B.; Skrabalak, S.E. Shape-controlled synthesis of metal nanocrystals: Simple chemistry meets complex physics? *Angew. Chem. Int. Ed.* **2009**, *48*, 60–103.
3. Li, Y.D.; Liu, L.P.; Zhuang, Z.B.; Xie, T.; Wang, Y.G.; Li, J.; Peng, Q. Shape control of CdSe nanocrystals with zinc blende structure. *J. Am. Chem. Soc.* **2009**, *131*, 16423–16429.
4. Cao, Y.C.; Yang, Y.A.; Wu, H.M.; Williams, K.R. Synthesis of CdSe and CdTe nanocrystals without precursor injection. *Angew. Chem. Int. Ed.* **2005**, *44*, 6712–6715.
5. Yang, H.B.; Sui, Y.M.; Fu, W.Y.; Zeng, Y.; Zhang, Y.Y.; Zhao, Q.; Li, Y.E.; Zhou, X.M.; Leng, Y.; Li, M.H.; Zou, G.T. Low temperature synthesis of $Cu_2O$ crystals: Shape evolution and growth mechanism. *Cryst. Growth Des.* **2010**, *10*, 99–108.
6. Wang, X.; Wu, H.F.; Kuang, Q.; Huang, R.B.; Xie, Z.X.; Zheng, L.S. Shape-dependent antibacterial activities of $Ag_2O$ polyhedral particles. *Langmuir* **2010**, *26*, 2774–2778.
7. McFarland, E.W.; Siripala, W.; Ivanovskaya, A.; Jaramillo, T.F.; Baeck, S.H. A $Cu_2O/TiO_2$ heterojunction thin film cathode for photoelectrocatalysis. *Sol. Energ. Mat. Sol. C* **2003**, *77*, 229–237.
8. Li, Y.D.; Zhang, J.T.; Liu, J.F.; Peng, Q.; Wang, X. Nearly monodisperse $Cu_2O$ and CuO nanospheres: Preparation and applications for sensitive gas sensors. *Chem. Mater.* **2006**, *18*, 867–871.

9.  Ho, J.Y.; Huang, M.H. Synthesis of submicrometer-sized Cu₂O crystals with morphological evolution from cubic to hexapod structures and their comparative photocatalytic activity. *J. Phys. Chem. C* **2009**, *113*, 14159–14164.

10. Tarascon, J.M.; Poizot, P.; Laruelle, S.; Grugeon, S.; Dupont, L. Nano-sized transition-metaloxides as negative-electrode materials for lithium-ion batteries. *Nature* **2000**, *407*, 496–499.

11. Pascual, J.I.; Mendez, J.; Gomezherrero, J.; Baro, A.M.; Garcia, N.; Landman, U.; Leudtke, W.D.; Bogachek, E.N.; Cheng, H.P. Electrical and mechanical-properties of metallic nanowires—Conductance quantization and localization. *J. Vac. Sci. Technol. B* **1995**, *13*, 1280–1284.

12. Hou, S.M.; Liu, H.W.; Zhang, G.M.; Shen, Z.Y.; Liu, W.M.; Wu, J.L.; Xue, Z.Q.; Roy, E.; Zhang, K.Y. Structure and electrical properties of gold nanowires grown with electrochemical deposition. *Acta Phys. Chim. Sin.* **2002**, *18*, 359–363.

13. Kim, J.R.; So, H.M.; Park, J.W.; Kim, J.J.; Kim, J.; Lee, C.J.; Lyu, S.C. Electrical transport properties of individual gallium nitride nanowires synthesized by chemical-vapor-deposition. *Appl. Phys. Lett.* **2002**, *80*, 3548–3550.

14. Liu, Z.; Searson, P.C. Electrical transport properties of nanoporous gold nanowires. *Abstr. Pap. Am. Chem. Soc.* **2004**, *228*, U878.

15. Biswas, K.; Qin, Y.; DaSilva, M.; Reifenberger, R.; Sands, T. Electrical properties of individual gold nanowires arrayed in a porous anodic alumina template. *Phys. Status. Solidi. A* **2007**, *204*, 3152–3158.

16. Tian, Y.; Liu, H.Q.; Deng, Z.F. Morphology-dependent electrochemistry and electrocatalytical activity of cytochrome C. *Langmuir* **2007**, *23*, 9487–9494.

17. Mekasuwandumrong, O.; Pisduangdaw, S.; Panpranot, J.; Methastidsook, C.; Chaisuk, C.; Faungnawakij, K.; Praserthdam, P. Characteristics and catalytic properties of Pt-Sn/Al₂O₃ nanoparticles synthesized by one-step flame spray pyrolysis in the dehydrogenation of propane. *Appl. Catal. Gen.* **2009**, *370*, 1–6.

18. Cuenya, B.R.; Mostafa, S.; Behafarid, F.; Croy, J.R.; Ono, L.K.; Li, L.; Yang, J.C.; Frenkel, A.I. Shape-dependent catalytic properties of pt nanoparticles. *J. Am. Chem. Soc.* **2010**, *132*, 15714–15719.

19. Switzer, J.A.; Liu, R.; Oba, F.; Bohannan, E.W.; Ernst, F. Shape control in epitaxial electrodeposition: Cu₂O nanocubes on InP(001). *Chem. Mater.* **2003**, *15*, 4882–4885.

20. Leung, K.T.; Radi, A.; Pradhan, D.; Sohn, Y. Nanoscale shape and size control of cubic, cuboctahedral, and octahedral Cu-Cu₂O core-shell nanoparticles on Si(100) by one-step, templateless, capping-agent-free electrodeposition. *ACS Nano* **2010**, *4*, 1553–1560.

21. Wong, P.K.; Yu, Y.; Du, F.P.; Yu, J.C.; Zhuang, Y.Y. One-dimensional shape-controlled preparation of porous Cu₂O nano-whiskers by using CTAB as a template. *J. Solid State Chem.* **2004**, *177*, 4640–4647.

22. Fan, W.Y.; Ng, C.H.B. Shape evolution of Cu₂O nanostructures via kinetic and thermodynamic controlled growth. *J. Phys. Chem. B* **2006**, *110*, 20801–20807.

23. Kamath, P.V.; Joseph, S. Electrochemical deposition of Cu₂O on stainless steel substrates: Promotion and suppression of oriented crystallization. *Solid State Sci.* **2008**, *10*, 1215–1221.

24. Fang, Z.; Lin, X.; Jian, X.; Wang, X.Y.; Wei, X.W.; Tao, F. Synthesis of Copper oxide hierarchical nanostructures. *Chin. J. Chem.* **2010**, *28*, 2377–2382.

25. Huang, M.H.; Kuo, C.-H. Morphologically controlled synthesis of $Cu_2O$ nanocrystals and their properties. *Nano Today* **2010**, *5*, 106–116.

26. Kuo, C.-H.; Huang, M.H. Facile synthesis of $Cu_2O$ nanocrystals with systematic shape evolution from cubic to octahedral structures. *J. Phys. Chem. C* **2008**, *112*, 18355–18360.

27. Huang, M.H.; Lin, P.-H. Shape-controlled synthesis of polyhedral nanocrystals and their facet-dependent properties. *Adv. Func. Mater.* **2012**, *22*, 14–24.

28. Huang, W.-C.; Lyu, L.-M.; Yang, Y.-C.; Huang, M.H. Synthesis of $Cu_2O$ Nanocrystals from cubic to rhombic dodecahedral structures and their comparative photocatalytic activity. *J. Am. Chem. Soc.* **2012**, *134*, 1261–1267.

29. Liu, X.-W. Selective growth of Au nanoparticles on (111) facets of $Cu_2O$ microcrystals with an enhanced electrocatalytic property. *Langmuir* **2011**, *27*, 9100–9104.

30. Kuo, C.-H.; Yang, Y.-C.; Gwo, S.; Huang, M.H. Facet-dependent and au nanocrystal-enhanced electrical and photocatalytic properties of Au-$Cu_2O$ core-shell heterostructures. *J. Am. Chem. Soc.* **2010**, *133*, 1052–1057.

31. Toghill, K.E.; Compton, R.G. Electrochemical non-enzymatic glucose sensors: A perspective and an evaluation. *Int. J. Electrochem. Sci.* **2010**, *5*, 1246–1301.

32. Xiao, F.; Zhao, F.; Mei, D.; Mo, Z.; Zeng, B. Nonenzymatic glucose sensor based on ultrasonic-electrodeposition of bimetallic PtM (M = Ru, Pd and Au) nanoparticles on carbon nanotubes-ionic liquid composite film. *Biosens. Bioelectron.* **2009**, *24*, 3481–3486.